International Journal For Advanced Research In Science & Technology
A peer reviewed international journal
www.ijarst.in
ISSN: 2457-0362

Simulation of Speed control of switched reluctance motor using ANFIS

1 K.Deepak,2A.Susmitha,3 R.Nandini,4 P.Srilakshmi,5 M.Sameera
1Assistant Professor,2,3,4,5B-tech student Scholar
1,2,3,4,5Department of Electrical & Electronics Engineering
1,2,3,4,5 G. Pullaiah College of Engineering and Technology, Nandikotkur Rd, near Venkayapalle, Pasupula Village, Kurnool, Andhra Pradesh 518002

Abstract —This paper develops an ANFIS based torque controlof SRM to reduce the torque ripple. The ANFIS has theadvantages of expert knowledge of the fuzzy inference systemand the learning capability of neural networks. This controllerrealizes a good dynamic behavior of the motor, a perfect speedtracking with no overshoot and a good rejection of impact loadsdisturbance. The results of applying the adaptive neuro-fuzzycontroller to a SRM give better performance and highrobustness than those obtained by the application of aconventional controller (PI). The above controller was realizedusing MATLAB/Simulink.

Index Terms— ANFIS, Torque Control, Switched ReluctanceMotor.

I. INTRODUCTION

Switched reluctance motor is an electric motor that runs by reluctance torque and The SRM is very attractive for many industrial applications due to its simple fabrication ,accuracy, rugged construction ,high torque, low cost ,simple structure due to absence of magnets , rotor conductors and brushes, low construction cost, high reliability, high power density, fast dynamic response, good controllability, fault tolerance, high efficiency, etc. because of this advantages, this motor have attracted many researches, especially at last two decades. One of the primarydisadvantages of the SRM is the high torque ripple. high torque ripple which contributes to acoustic noise and vibration. The origin of torque pulsations is due to the non-linear and discrete nature of the torque production mechanism. Minimization of torque ripple is essential for high performance. The performance of SRM is depends on its design. It can be reduced by machine design or by control circuits. Conventionally, SRM is driven by asymmetric half bridges and there are three main control methods for SRM: single pulse operation, chopping-voltage PWM, and chopping-current regulation. Single pulse operation is usually used in high-speed operation.

Chopping-voltage PWM method is equivalent to reduced dc voltage signal pulse operation. In order to reduce the torque ripple at low speed, chopping current regulation is generally used.
A 8/6 poles SR motor. It is doubly salient and has no rotor windings. The torque in this motor is due to the tendency of rotor poles to align with the poles of exited stator phase. The direction of the torque is independent of the direction of the phase current. The phases are critically fed by unipolar currents to get unidirectional torque. A shaft position sensor is used to facilitate the turn on and off of the phase windings.

Fig.1 shows a typical control diagram for SRM driven by asymmetric half bridges. Current controller is employed to generate switching signals for the asymmetric half bridges according to the current reference. The current reference is either given by a speed controller or a torque distributer. If the current reference comes directly from a speed controller, flat top chopping current for each phase is employed. Due to the strong nonlinearity, in some cases, the flat top chopping current regulation might not provide satisfactory performance. Therefore, torque sharing control is used to distribute torque production between two phases in order to produce constant torque [2][7].

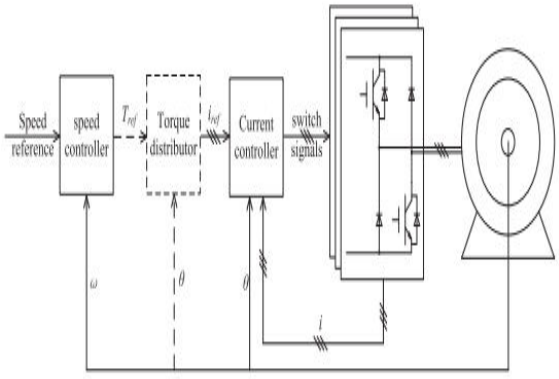

Fig.1. Typical SRM control diagram

Both flat top chopping current regulation and torque sharingcontrol rely on accurate current

International Journal For Advanced Research In Science & Technology
A peer reviewed international journal www.ijarst.in
ISSN: 2457-0362

controllers. Hysteresis control is one of the most popular current control schemes in SRMs,due to its fast dynamic response and model independency [4]–[8]. However, hysteresis controller also suffers from drawbacks including variable switching frequency and very high sampling rate [9]-[11]. Variable switching frequency in hysteresis control makes it difficult to design the electromagnetic interference(EMI) filter and may cause an acoustical noise. High-speedADCs have higher samplingrate, however, they add additional cost to the SRM drive system.

In order to avoid the drawbacks of the hysteresis current controller, fixed frequency PWM controllers have been studied[9], [11]–[16]. In [12], an open loop PWM controller is used, whereas in [9], a proportional-integral (PI) current controller has been investigated and a current sampling method for digital control have been introduced. A proportional (P) controller with an iterative learning control is proposed in [17] to achieve accurate current control. In [11], [13]-[16], back EMF compensation to the PI current controller has been analyzed. In [11],the gains of the PI controller are adjusted according to current and rotor position. However, a PI controller suffers from either slow response or possible overshot. It is also difficult to tune thePI controller in SRM applications due to the highly nonlinear characteristics of the machine.

Model-based dead-beat flux controller are proposed in [18]-[21]. The dead-beat controller achieves constant switching frequency and lower sampling rate, while maintaining the similar dynamic response as hysteresis controller. However, the performance of a dead-beat controller relies on an accurate model and a large gain, which may degrade the performance of the dead-beat controller.

In [22], a Lyapunov function-based controller is proposed to solve model mismatch issue. The tracking error is bounded by the parameters of the controller. A sliding mode current controller is proposed in [23]. Parameters of these controllers are carefully selected according to the model mismatch. These control methods need to store several look-up tables, which increase the storage and computational burden of the digital controller.

A digital PWM current controller for the SRM drives is proposed in this paper in order to achieve fast response, accurate tracking, immunity to noise, model mismatch, and stability. The proposed controller takes full advantage of the model information. Smaller feedback gain could be chosen in order to reduce noise sensibility without degrading the performance. Parameter adaption is adopted to deal with the model mismatch. Relationships between the proposed controller and the previous mentioned PI dead-beat controllers are discussed. Both the simulation and experimental results are provided to verify the performance of the proposed current controller.

(II) MODEL OF SRM

By neglecting mutual coupling between phases, the phase voltage equation of an SRM can be given as

$$u_w = R_w \cdot i + \frac{d\psi(\theta, i)}{dt} \tag{1}$$

Where*uw*is the phase voltage applied on the phase winding, Rw is the winding resistance, ψ is the flux linkage, θ is the rotor position, and *i*is the phase current.

Due to its double salient structure and saturation, ψ is a nonlinear function of both i and θ. Fig. 2 shows the measured flux linkage profile of the SRM studied in this paper. The rotor spins360◦ per electric period. The aligned positions are 0◦ and 360◦.The unaligned position is 180◦. Fig. 2 could be stored into a lookup table when digital control is applied.

Considering the modeling errors, the real flux linkage is represented as

$$\psi(\theta, i) = \alpha\psi_m(\theta, i) \tag{2}$$

where is the modeled flux linkage profile used in the controller, and factor α is a positive number that donates the relationship between the modeled flux linkage profile and the real one.

In the ideal case, the modeled flux linkage profile exactly matches the real one, and α = 1. But in practice, no matter whether ψm is obtained by the experimental measurement or by an FEA calculation, there may be some mismatch between ψ and ψm. In this case, ψm is unknown and α may be variable and there is

$$\begin{aligned} \alpha &> 0 \\ \bar{\alpha} - B_\alpha \le \alpha &\le \bar{\alpha} + B_\alpha \\ |\dot{\alpha}| &\le B_{\dot{\alpha}} \end{aligned} \tag{3}$$

where $\bar{\alpha}$ is the average value of α, Bα ≥ 0 is the variation bound of α, and Bα ˙ ≥ 0 is the maximum variation rate of α. The values of Bα and Bα ˙ depend on the modeling errors of thestudied motor.

International Journal For Advanced Research In Science & Technology
A peer reviewed international journal www.ijarst.in
IJARST
ISSN: 2457-0362

Considering the resistances and voltage drops on windings and switches, the phase voltage equation could be written as

$$\frac{d\psi_m(\theta,i)}{dt} = -\frac{1}{\alpha}(R_w+R_c)\,i - \frac{1}{\alpha}\left(\psi_m(\theta,i)\frac{d\alpha}{dt} + v_c + v_m + v_n\right) + \frac{1}{\alpha}u_c \tag{4}$$

where uc donates the converter output voltage, Rc donates the equivalent resistance of the converter,Rc could be obtained from either experiments or data sheets, but it changes according to current, temperature, gate source (GS) voltage, etc. vc donates the voltage drop on the converter, vm donates the voltage drop caused by mutual inductance, vn reflects all other voltage drops, and noises in the system. Equation (4) could be formulated as

$$\begin{aligned}\frac{d\psi_m(\theta,i)}{dt} &= -\frac{1}{\alpha}Ri - \frac{1}{\alpha}v + \frac{1}{\alpha}u_c\\ R &= R_w + R_c\\ v &= \psi_m(\theta,i)\frac{d\alpha}{dt} + v_c + v_m + v_n\end{aligned} \tag{5}$$

where R is the total equivalent resistance and v is the total equivalent voltage drop. They are uncertain parameters that are not easy to model. The values of R and v are both unknown and may be variable, which are represented as

$$\begin{aligned}Ra &> 0\\ \bar{R} - B_R \le\ & R \le \bar{R} + B_R\\ |\dot{R}| &\le B_{\dot{R}}\\ \bar{v} - B_v \le\ & v \le \bar{v} + B_v\\ |\dot{v}| &\le B_{\dot{v}}\end{aligned} \tag{6}$$

where $\bar{R}$ donates the average value of R, BR ≥ 0 donates thevariation bound of R, and Bv˙ ≥ 0 donates the maximum variation rate of R. R is also positive. $\bar{v}$donates the average value ofv, Bv˙ ≥ 0 donates the variation bound of v, and Bv˙ ≥ 0 donatesthe maximum variation rate of v.

(III) Proposed Current Controller

A current controller can either control the current directly or control the current indirectly by controlling the flux linkage. For a certain position θ, ψ is a monotone increasing function of i. For any i1 ≥ 0, i2 ≥ 0 there is

$$\begin{aligned}\psi_m(\theta,i_1) &> \psi_m(\theta,i_2) \Leftrightarrow i_1 > i_2\\ \psi_m(\theta,i_1) &= \psi_m(\theta,i_2) \Leftrightarrow i_1 = i_2\\ \psi_m(\theta,i_1) &< \psi_m(\theta,i_2) \Leftrightarrow i_1 < i_2\end{aligned} \tag{7}$$

Therefore, the phase current can be controlled by controlling its corresponding flux linkage. The SRM model shown in (4) contains unknown parameters, a current controller with estimated parameter values could be constructed as

$$u_c = \hat{\alpha}\frac{d\psi_m(\theta,i_{\text{ref}})}{dt} + \hat{R}i_{\text{ref}} + \hat{v} + ke \tag{8}$$

where ψm(θ,iref) is the reference flux linkage calculated by the reference current iref and rotor position θ, $\hat{\alpha}$ is the estimatedvalue of α, $\hat{R}$ is the estimated value of R, $\hat{v}$ is the estimatedvalue of v, k is a positive constant, and e is the flux linkage errorwhich can be expressed as

$$e = \psi_m(\theta,i_{\text{ref}}) - \psi_m(\theta,i) \tag{9}$$

Substituting (8) into (5), the flux linkage error dynamics canbe derived as

$$\begin{aligned}\dot{e} &= -\frac{k}{\alpha}e - \hat{R}e_i + \frac{1}{\alpha}\tilde{\alpha}\dot{\psi}_m(\theta,i_{\text{ref}}) + \frac{1}{\alpha}\tilde{R}i + \frac{1}{\alpha}\tilde{v}\\ \tilde{\alpha} &= \alpha - \hat{\alpha}\\ \tilde{R} &= R - \hat{R}\\ \tilde{v} &= v - \hat{v}\\ e_i &= i_{\text{ref}} - i\end{aligned} \tag{10}$$

where $\tilde{\alpha}$, $\tilde{R}$and $\tilde{v}$ are the estimation errors, ei is the currenterror.

If a Lyapunov candidate is selected as

$$V = \frac{1}{2}e^2 + \frac{1}{2\alpha k_\alpha}\tilde{\alpha}^2 + \frac{1}{2\alpha k_R}\tilde{R}^2 + \frac{1}{2\alpha k_v}\tilde{v}^2 \tag{11}$$

where kα, kR, and kv are positive constants. Then, the derivative of the Lyapunov candidate is

$$\begin{aligned}\dot{V} = & -\frac{k}{\alpha}e^2 - \frac{\tilde{R}}{\alpha}ee_i\\ & + \frac{1}{\alpha}\tilde{\alpha}\dot{\psi}_m(\theta,i_{\text{ref}})e - \frac{1}{\alpha k_\alpha}\tilde{\alpha}\dot{\hat{\alpha}}\\ & + \frac{1}{\alpha}\tilde{R}ie - \frac{1}{\alpha k_R}\tilde{R}\dot{\hat{R}}\\ & + \frac{1}{\alpha}\tilde{v}e - \frac{1}{\alpha k_v}\tilde{v}\dot{\hat{v}}\\ & + \frac{\tilde{\alpha}\dot{\alpha}}{\alpha k_\alpha} + \frac{\tilde{R}\dot{R}}{\alpha k_R} + \frac{\tilde{v}\dot{v}}{\alpha k_v}.\end{aligned} \tag{12}$$

International Journal For Advanced Research In Science & Technology
A peer reviewed international journal
www.ijarst.in
ISSN: 2457-0362

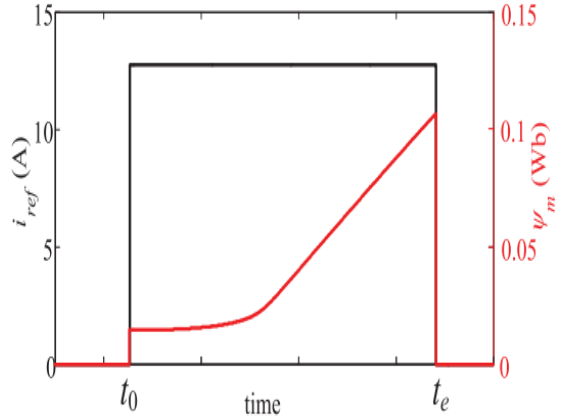

Fig. 2.Typical waveform of ψm (θ, iref) and iref

It can be seen from (12) that if $\hat{\alpha}$,$\hat{R}$, and $\hat{v}$are chosen as

$$\dot{\hat{\alpha}} = k_\alpha \dot{\psi}_m(\theta, i_{\text{ref}})e$$
$$\dot{\hat{R}} = k_R ie$$
$$\dot{\hat{v}} = k_v e.$$

(13)

Then, (12) becomes

$$\dot{V} = -\frac{k}{\alpha}e^2 - \frac{\hat{R}}{\alpha}ee_i + \frac{\tilde{\alpha}\dot{\alpha}}{\alpha k_\alpha} + \frac{\tilde{R}\dot{R}}{\alpha k_R} + \frac{\tilde{v}\dot{v}}{\alpha k_v}$$

(14)

(A) Constant Parameters

k, $\hat{R}$, and α are positive constants, and according to (7), eiand e have the same sign. If α, R, v are constant, i.e.,

$$\dot{\alpha} = 0, \dot{R} = 0, \dot{v} = 0$$

(15)

$\dot{V}$becomes

$$\dot{V} = -\frac{k}{\alpha}e^2 - \frac{\hat{R}}{\alpha}ee_i$$

Therefore˙ is semi negative definite. This indicates that the system is globally asymptotically stable, and e is going to converge to zero. If e converges to zero, the system is internally stable. The convergence rate of e is determined by k and α. Since αis around 1, k could be selected to adjust the convergence rate. According to (16), a larger k gives a faster convergence rate, which means faster dynamic response. However, according to(8), k is the feedback gain of the error, in this case, a large gain means that the controller is more sensitive to noise. Therefore, the selection of k is a tradeoff between the dynamic response and robustness. According to (10), if e converges to zero, forany ψ ˙m(θ,iref) and i, there will be

$$\tilde{\alpha}\dot{\psi}_m(\theta, i_{\text{ref}}) + \tilde{R}i + \tilde{v} = 0$$

(17)

As is known, the adaptive controllers suffer from parameter drafting. Since all the estimated parameters are bounded, the controller will be stable. However, parameters will not necessarily converge to their real values unless persistent excitation condition is satisfied [24]. For the case of (13), ψ ˙m (θ,iref) andi need to be "rich" enough to guarantee the convergence. Fig. 3shows a typical waveform of ψm (θ,iref) and iref with flat-top current control. It can be seen that iref is a constant number andi˙ref is zero, while ψm (θ,iref) is a nonlinear function of time.

The nonlinearity of ψm (θ,iref) will provide sufficient frequencies to make ψ ˙m (θ,iref) "rich." This is another reason why flux linkage is selected to be controlled instead of current. In this case, there is

$$\Psi(t) = \left[\dot{\psi}_m(\theta, i_{\text{ref}}, t), 1\right]^T$$
$$\int_{t_o}^{t_e} \Psi(\tau)\Psi(\tau)^T d\tau \geq \gamma I$$

(18)

where t_0 is the beginning of each stroke and te is the end of the stroke. Equation (18) indicates that Ψ (t) satisfies the exciting condition, which means $||[\tilde{\alpha}\tilde{v}]||_2$ is going to converge perstoke [24]. In this case, as the controller is active each stroke, the estimation errors are going to converge to zero eventuallyand there will be

$$\hat{\alpha} = \alpha$$
$$\hat{v} = v$$

(19)

However, if the flat-top current control is applied, i may not be rich enough to guarantee the convergence of $\hat{R}$. In this case, adead zone should be added to prevent parameter drafting of $\hat{R}$.

(B) Variable Parameters

Practically, the parameters α, R, and v are not constant

$$\dot{\alpha} \neq 0, \dot{R} \neq 0, \dot{v} \neq 0$$

(20)

Since α, R, and v have their own bounds, the adaption law in(13) should be modified by

International Journal For Advanced Research In Science & Technology
A peer reviewed international journal www.ijarst.in
IJARST
ISSN: 2457-0362

$$\dot{\hat{\alpha}} = \begin{cases} k_\alpha \dot{\psi}_m(\theta, i_{\text{ref}})e, \ \hat{\alpha} \in [\bar{\alpha} - B_\alpha, \bar{\alpha} + B_\alpha] \\ k_\alpha \dot{\psi}_m(\theta, i_{\text{ref}})e, \ \hat{\alpha} > \bar{\alpha} + B_\alpha \text{ and } \dot{\psi}_m(\theta, i_{\text{ref}})e < 0 \\ k_\alpha \dot{\psi}_m(\theta, i_{\text{ref}})e, \ \hat{\alpha} < \bar{\alpha} - B_\alpha \text{ and } \dot{\psi}_m(\theta, i_{\text{ref}})e > 0 \\ 0, \text{ else} \end{cases}$$

$$\dot{\hat{R}} = \begin{cases} k_R ie, \ \hat{R} \in [\bar{R} - B_R, \bar{R} + B_R] \\ k_R ie, \ \hat{R} > \bar{R} + B_R \text{ and } ie < 0 \\ k_R ie, \ \hat{R} < \bar{R} - B_R \text{ and } ie > 0 \\ 0, \text{ else} \end{cases}$$

$$\dot{\hat{v}} = \begin{cases} k_v e, \ \hat{v} \in [\bar{v} - B_v, \bar{v} + B_v] \\ k_v e, \ \hat{v} > \bar{v} + B_v \text{ and } e < 0 \\ k_v e, \ \hat{v} < \bar{v} - B_v \text{ and } e > 0 \\ 0, \text{ else.} \end{cases}$$

(21)

This modification does not affect the system stability if the real values of α, R, and v do not exceed their bounds. At the same time, (22) defines the bounds of parameter estimation error

$$|\tilde{\alpha}| \le 2B_\alpha, \left|\tilde{R}\right| \le 2B_R, |\tilde{v}| \le 2B_v$$

(22)

Combined with (3) and (6), there are

$$\frac{\tilde{\alpha}^2}{2\alpha k_\alpha} + \frac{\tilde{R}^2}{2\alpha k_R} + \frac{\tilde{v}^2}{2\alpha k_v} \le \frac{2B_\alpha^2}{\alpha k_\alpha} + \frac{2B_R^2}{\alpha k_R} + \frac{2B_v^2}{\alpha k_v} = M$$

(23)

$$\frac{\tilde{\alpha}\dot{\alpha}}{\alpha k_\alpha} + \frac{\tilde{R}\dot{R}}{\alpha k_R} + \frac{\tilde{v}\dot{v}}{\alpha k_v} \le \frac{2B_\alpha B_{\dot{\alpha}}}{\alpha k_\alpha} + \frac{2B_R B_{\dot{R}}}{\alpha k_R} + \frac{2B_v B_{\dot{v}}}{\alpha k_v} = N$$

(24)

where B$\dot{\alpha}$, B$\dot{R}$, and B$\dot{v}$ are the bounds of $\dot{\alpha}$, $\dot{R}$, and $\dot{v}$, respectively. According to (14) and (11), there is

$$e^2 = 2V - \frac{\tilde{\alpha}^2}{\alpha k_\alpha} - \frac{\tilde{R}^2}{\alpha k_R} - \frac{\tilde{v}^2}{\alpha k_v}$$

$$\dot{V} = -2\frac{k + k_i\hat{R}}{\alpha}\left(V - \frac{\tilde{\alpha}^2}{2\alpha k_\alpha} - \frac{\tilde{R}^2}{2\alpha k_R} - \frac{\tilde{v}^2}{2\alpha k_v}\right) + \frac{\tilde{\alpha}\dot{\alpha}}{\alpha k_\alpha} + \frac{\tilde{R}\dot{R}}{\alpha k_R} + \frac{\tilde{v}\dot{v}}{\alpha k_v}$$

(25)

Whereki> 0 donates the relationship between e and ei. According to (25), if V exceeds αN/2(k + ki$\hat{R}$) + M, $\dot{V}$ will benegative, and V is going to decrease. Thus, the control error isbounded by

$$|e| \le \sqrt{\alpha N/2(k + k_i\hat{R})} = \sqrt{\frac{2B_\alpha B_{\dot{\alpha}}}{(k + k_i\hat{R})k_\alpha} + \frac{2B_R B_{\dot{R}}}{(k + k_i\hat{R})k_R} + \frac{2B_v B_{\dot{v}}}{(k + k_i\hat{R})k_v}}$$

(26)

As shown from (26), for the predefined bounds and maximum variation rates of the unknown parameter, the control error is limited by k ,kα, kR , and kv.

(C) Digital Implementation of Proposed Current Controller

In digital implementation, the discrete form of (8) and (21)can be reformulated as

$$\Delta\psi_m(k) = \psi_m(\theta(k+1), i_{\text{ref}}(k+1)) - \psi_m(\theta(k), i_{\text{ref}}(k))$$

$$u_c(k) = \hat{\alpha}(k)\frac{\Delta\psi_m(k)}{T} + \hat{R}(k)i_{\text{ref}}(k) + \hat{v}(k) + ke(k)$$

(27)

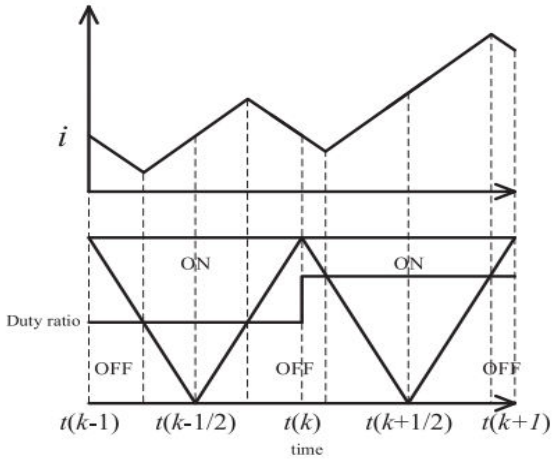

Fig. 3. PWM modulation

Where$T$ is the digital sampling time, $\theta(k + 1) = \theta(k) + \omega T$,and ω is the electric angular speed of the SRM

$$\hat{\alpha}(k+1)' = \hat{\alpha}(k) + k_\alpha \Delta\psi_m(k)\, e(k)$$

$$\hat{\alpha}(k+1) = \begin{cases} \hat{\alpha}(k+1)', \ \hat{\alpha}(k+1)' \in [\bar{\alpha} - B_\alpha, \bar{\alpha} + B_\alpha] \\ \bar{\alpha} + B_\alpha, \ \hat{\alpha}(k+1)' > \bar{\alpha} + B_\alpha \\ \bar{\alpha} - B_\alpha, \ \hat{\alpha}(k+1)' < \bar{\alpha} - B_\alpha \end{cases}$$

$$e(k)' = \begin{cases} e(k), |e(k)| > B_{DZ} \\ 0, |e(k)| \le B_{DZ} \end{cases}$$

$$\hat{R}(k+1)' = \hat{R}(k) + k_R i(k)\, e(k)\, T$$

$$\hat{R}(k+1) = \begin{cases} \hat{R}(k+1)', \ \hat{R}(k+1)' \in [\bar{R} - B_R, \bar{R} + B_R] \\ \bar{R} + B_R, \ \hat{R}(k+1)' > \bar{R} + B_R \\ \bar{R} - B_R, \ \hat{R}(k+1)' < \bar{R} - B_R \end{cases}$$

$$\hat{v}(k+1)' = \hat{v}(k) + k_v e(k)\, T$$

$$\hat{v}(k+1) = \begin{cases} \hat{v}(k+1)', \ \hat{v}(k+1)' \in [\bar{v} - B_v, \bar{v} + B_v] \\ \bar{v} + B_v, \ \hat{v}(k+1)' > \bar{v} + B_v \\ \bar{v} - B_v, \ \hat{v}(k+1)' < \bar{v} - B_v \end{cases}$$

(28)

WhereΔψm(k) is defined in (27). BDZ is the error dead zone,$\bar{\alpha}$, $\bar{R}$, and $\bar{v}$ are the estimated average values of α, R, and v,respectively.

(IV)PWM Delay Compensation

Fig..3 shows the PWM modulation for digital control. Theduty ratio is either obtained by *uc/UDC* for soft chopping or0.5 + 0.5(*uc/UDC*) for hard chopping. *UDC* is the dc bus voltage. In the *k*th control period, current should be sampled at*t*(*k*). But in practice, especially in a DSP control, if currentis sampled at *t*(*k*), it will take some time for the controller to calculate the duty ratio and the duty ratio for *t*(*k*) is actuallyloaded into the PWM modulator at *t*(*k* + 1).

International Journal For Advanced Research In Science & Technology
A peer reviewed international journal
www.ijarst.in
ISSN: 2457-0362

This brings one sampling time delay into the control loop. In this case, the dutyratio for $t(k)$ should be calculated before $t(k)$. Mohamed andEl-Saadany [10] proposes a predictive current controller to solve

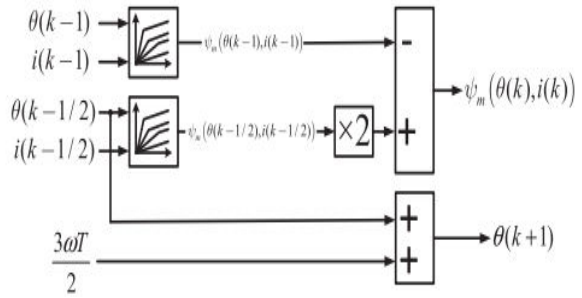

Fig. 4. Approximation of i(k), θ(k), and θ(k + 1)

the problem. However, the predictive current controller needsaccurate model and increases the calculation burden for DSP,especially for nonlinear systems such as SRMs. Blaabjergetal.[9] recommends that current should be sampled at t(k − 1/2),which means i(k) is approximated by

$$i(k) \approx i(k-1/2) \tag{29}$$

As shown in Fig. 3, there is no switching action at t(k − 1/2),EMI noise at that instance can be avoided. Furthermore, the duty ratio can be calculated within half of the period and delay in thecontrol loop is avoided.

The estimation of (29) is accurate if the average current of each kth period stays the same, as the (k − 1) th period shown in Fig. 3. If average current between each period changes, as thekth period shown in Fig.4, (29) is not accurate.

As shown in Fig. 3, with the symmetrical modulation, the voltage waveforms of the former half period and the latter halfperiod are symmetric. Therefore, the flux could be estimatedinstead of current. The flux ψm (θ(k),i(k)) could be approximated by

$$\psi_m\left(\theta(k), i(k)\right) \approx 2\psi_m\left(\theta(k-1/2), i(k-1/2)\right) - \psi_m\left(\theta(k-1), i(k-1)\right). \tag{30}$$

In (30), current is sampled at both $t(k - 1/2)$ and $t(k - 1)$,which doubles the sampling rate. The ADCs used in motor control is capable of working at the sampling rate of twice of the PWM frequency without increasing any cost. Similar to(29), (30) also avoids the EMI noise caused by the switching action, provides half control period for duty ratio calculation, and avoids the delay in the control loop as well. Since the current sampling, and other calculations are performed at $t(k - 1/2)$, the rotor position also has to be approximated with the information at $t(k - 1/2)$. Fig. 4 shows the approximation of $\psi m(\theta(k),i(k))$ and $\theta(k + 1)$ for further use.

(A) Flux Reference Adjustment

When implemented in a digital processor, the current controller has to meet physical limits. Normally, when a phase isturned ON, the phase current is expected to rise quickly to the reference value, however, the voltage applied on the phase is limited by UDC. It is necessary to adjust (θ(k + 1),iref(k + 1))

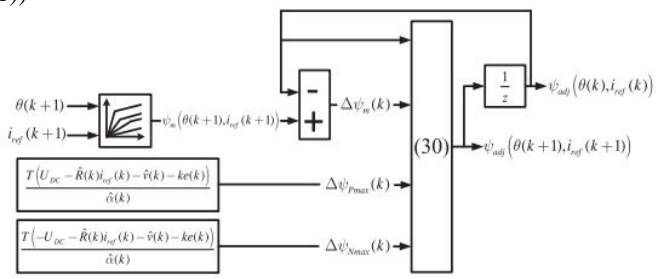

Fig. 5. Procedure of calculating ψadj (θ(k + 1), iref (k + 1)) andψadj (θ(k), iref (k)).

so that uc(k) would not exceed UDC

$$\Delta\psi_m(k) = \psi_m\left(\theta(k+1), i_{\text{ref}}(k+1)\right) - \psi_{\text{adj}}\left(\theta(k), i_{\text{ref}}(k)\right)$$

$$\Delta\psi_{P\max}(k) = \frac{T\left(U_{DC} - \hat{R}(k)i_{\text{ref}}(k) - \hat{v}(k) - ke(k)\right)}{\hat{\alpha}(k)}$$

$$\Delta\psi_{N\max}(k) = \frac{T\left(-U_{DC} - \hat{R}(k)i_{\text{ref}}(k) - \hat{v}(k) - ke(k)\right)}{\hat{\alpha}(k)}$$

$$\psi_{\text{adj}}\left(\theta(k+1), i_{\text{ref}}(k+1)\right) = \psi_{\text{adj}}\left(\theta(k), i_{\text{ref}}(k)\right) + \begin{cases} \Delta\psi_{P\max}(k), & \Delta\psi_m(k) > \Delta\psi_{P\max}(k) \\ \Delta\psi_{N\max}(k), & \Delta\psi_m(k) < \Delta\psi_{N\max}(k) \\ \Delta\psi_m(k), & \Delta\psi_{N\max}(k) \le \Delta\psi_m(k) \le \Delta\psi_{P\max}(k). \end{cases} \tag{31}$$

Therefore, ψm (θ(k + 1),iref(k + 1)) and ψm (θ(k),iref(k))in (27) should be replaced by ψadj (θ(k + 1),iref(k + 1)) andψadj (θ(k),iref(k)), respectively. Fig. 5 shows the procedure of calculatingψadj (θ(k + 1),iref(k + 1)) and ψadj (θ(k),iref(k))according to (31). Fig. 6 shows the procedure of calculating, α ˆ(k), R ˆ(k), and v ˆ(k) according to (28). Fig. 7 shows the procedure of calculating uc(k) according to (27).

(B). Relationship With Previously Proposed Controllers

As shown in Fig. 7, the controller of (27) consists of two parts: the feedback part and the feed forward part. The feedback part is sensitive to noise, while the feed forward part is immune to noise. In order to enhance the robustness of the controller, thefeed forward part should give out most part of uc so that less control effort is needed by the feedback part.

The digital controller of (27) has similar form with previously proposed controllers. For

International Journal For Advanced Research In Science & Technology
A peer reviewed international journal
www.ijarst.in
ISSN: 2457-0362

example, all the estimated parameters are taken as its real value, and k = 1/T, then (27) becomes

$$u_c(k) = \frac{\psi_m\left(\theta(k+1), i_{\text{ref}}(k+1)\right) - \psi_m\left(\theta(k), i(k)\right)}{T} + Ri(k) + v. \tag{32}$$

This is a typical dead-beat controller proposed in [18]-[21]. If $\hat{\alpha}$ is fixed as Kp · T and only the adaption of $\hat{v}$ is active with a

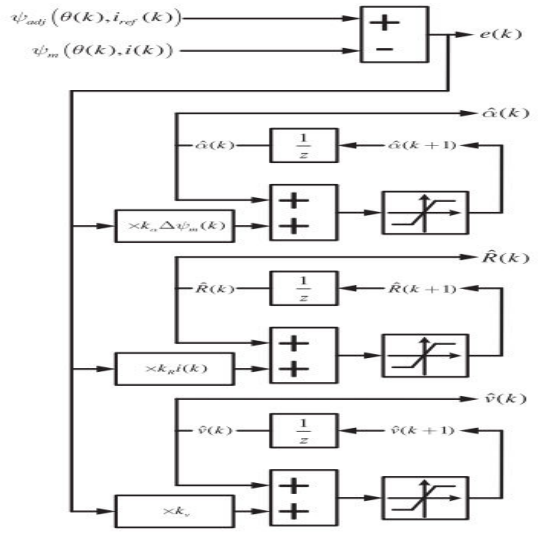

Fig.6. Procedure of calculating e, $\hat{\alpha}$ (k), $\hat{R}$ (k), and $\hat{v}$ (k)

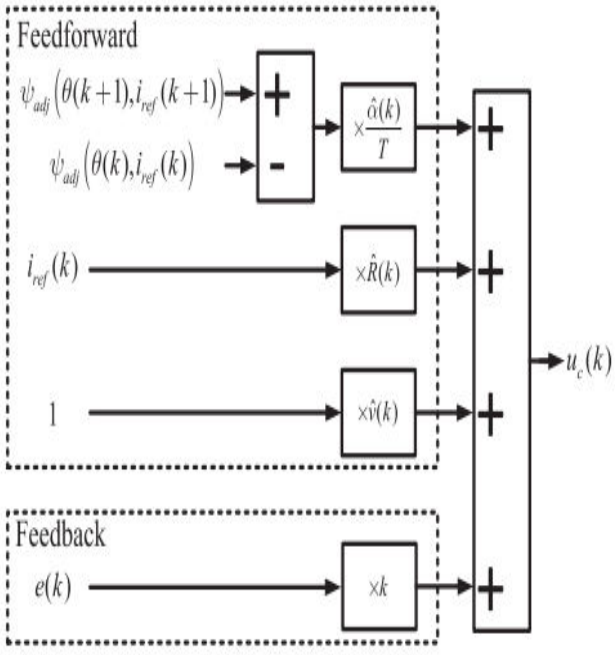

Fig. 7. Procedure of calculating uc(k)

gain of Ki, then (27) becomes a PI controller

$$\begin{aligned} u_c(k) = {} & K_p\left(\psi_m\left(\theta(k+1), i_{\text{ref}}(k+1)\right)\right. \\ & \left. -\psi_m\left(\theta(k), i(k)\right)\right) + Ri(k) + \hat{v}(k) \\ \hat{v}(k+1) = {} & \hat{v}(k) + K_i e(k) T. \end{aligned} \tag{33}$$

From this point of view, the proposed controller could be regarded as the improvement of some of the existing controllers.

(D) Parameter Selection

With the digital controller in (27), the error transfer function(10) could be rewritten in discrete domain as

$$\begin{aligned} e(k+2) = {} & \left(1 - \frac{k}{\alpha}T\right) e(k+1) - \hat{R}(k+1) T e_i(k+1) \\ & + \frac{1}{\alpha}\tilde{\alpha}(k+1)\Delta\psi_{\text{adj}}\left(\theta(k+1), i_{\text{ref}}(k+1)\right) \\ & + \frac{1}{\alpha}T\tilde{R}(k+1) i(k+1) + \frac{1}{\alpha}T\tilde{v}(k+1) \end{aligned} \tag{34}$$

Since the sampling time T is usually small enough, substituting(28) into (34), the error dynamics can be obtained as

$$\begin{aligned} & ez^2 - \left(1 - \frac{k}{\alpha}T\right) ez + Pe = O \\ & P = k_\alpha \frac{\Delta\psi_{\text{adj}}\left(\theta(k), i_{\text{ref}}(k)\right) \Delta\psi_{\text{adj}}\left(\theta(k+1), i_{\text{ref}}(k+1)\right)}{\alpha} \\ & \quad + k_R \frac{i(k+1) i(k)}{\alpha} T^2 + k_v \frac{1}{\alpha} T^2 \end{aligned} \tag{35}$$

where O is small enough bounded items, which could be taken as input of the error dynamic. The poles of the discrete transfer function of (35) are

$$\lambda_{1,2} = \frac{\left(1 - \frac{k}{\alpha}T\right) \pm \sqrt{\left(1 - \frac{k}{\alpha}T\right)^2 - 4P}}{2} \tag{36}$$

To stabilize the system, the poles should be placed inside the unit cycle, and hence the limits of the parameters are

$$\begin{aligned} 0 < {} & \frac{k}{\alpha}T < 2 + P \\ 0 < {} & P < \frac{1}{4} \end{aligned} \tag{37}$$

It can be seen that in (32), k is selected to be 1/T and P is selected to be zero, and therefore, the poles are placed at zero. Due to the feed forward part in the proposed controller, a smaller could be chosen. After

International Journal For Advanced Research In Science & Technology
A peer reviewed international journal www.ijarst.in
ISSN: 2457-0362

k is chosen, kα, kR, and kv are selected to ensure the stability.

(V) ANFIS CONTROLLER

(A) Adaptive Neuro-Fuzzy Inference Systems: (ANFIS):

An adaptive neuro-fuzzy inference system or adaptive network-based fuzzy inference system (ANFIS) is a kind of artificial neural network that is based on Takagi–Sugeno fuzzy inference system. The technique was developed in the early 1990s. Since it integrates both neural networks and fuzzy logic principles, it has potential to capture the benefits of both in a single framework. Its inference system corresponds to a set of fuzzy IF–THEN rules that have learning capability to approximate nonlinear functions. Hence, ANFIS is considered to be a universal estimator. For using the ANFIS in a more efficient and optimal way, one can use the best parameters obtained by genetic algorithm.

The adaptive network based fuzzy inference system (ANFIS) is a data driven procedure representing a neural network approach for the solution of function approximation problems. Data driven procedures for the synthesis of ANFIS networks are typically based on clustering a training set of numerical samples of the unknown function to be approximated. Since introduction, ANFIS networks have been successfully applied to classification tasks, rule-based process control, pattern recognition and similar problems. Here a fuzzy inference system comprises of the fuzzy model proposed by Takagi, Sugeno and Kang to formalize a systematic approach to generate fuzzy rules from an input output data set.

(B)ANFIS structure

For simplicity, it is assumed that the fuzzy inference system under consideration has two inputs and one output. The rule base contains the fuzzy if-then rules of Takagi and Sugeno's type as follows:

If x is A and y is B then z is f(x,y)

where A and B are the fuzzy sets in the antecedents and z = f(x, y) is a crisp function in the consequent. Usually f(x, y) is a polynomial for the input variables x and y. But it can also be any other function that can approximately describe the output of the system within the fuzzy region as specified by the antecedent. When f(x,y) is a constant, a zero order Sugeno fuzzy model is formed which may be considered to be a special case of Mamdani fuzzy inference system where each rule consequent is specified by a fuzzy singleton. If f(x,y) is taken to be a first order polynomial a first order Sugenofuzzy model is formed. For a first order two rule Sugeno fuzzy inference system, the two rules may be stated as:

Rule 1: If x is A_1 and y is B_1 then $f_1 = p_1x + q_1y + r_1$

Rule 2: If x is A_2 and y is B_2 then $f_2 = p_2x + q_2y + r_2$

Here type-3 fuzzy inference system proposed by Takagi and Sugeno is used. In this inference system the output of each rule is a linear combination of the input variables added by a constant term. The final output is the weighted average of each rule's output. The corresponding equivalent ANFIS structure is shown in Fig. 8.

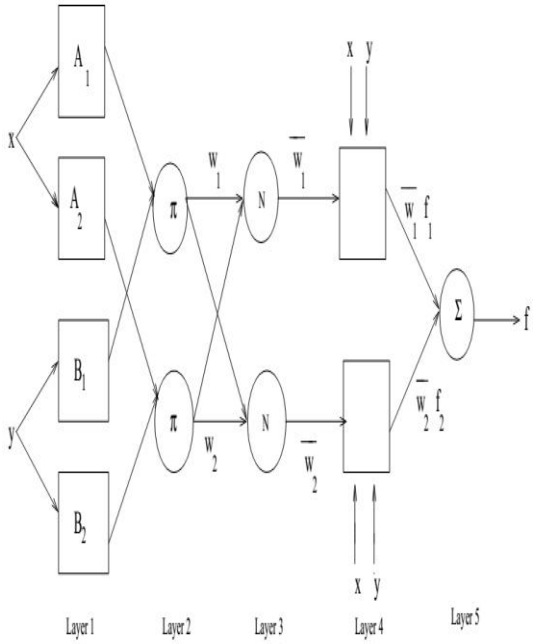

Fig. 8. Type-3 ANFIS Structure

The individual layers of this ANFIS structure are described below:

Layer 1: Every node i in this layer is adaptive with a node function

$$O_i^1 = \mu_{A_i}(x) \tag{38}$$

where, x is the input to node i, Ai is the linguistic variable associated with this node function and μAi is the membership function of Ai. Usually μAi(x) is chosen as

$$\mu_{A_i}(x) = \frac{1}{1 + [(\frac{x - c_i}{a_i})^2]^{b_i}} \tag{39}$$

International Journal For Advanced Research In Science & Technology
A peer reviewed international journal
www.ijarst.in
ISSN: 2457-0362

$$\mu_{A_i}(x) = exp\{-(\frac{x - c_i}{a_i})^2\} \quad (40)$$

where x is the input and {ai, bi, ci} is the premise parameter set.

Layer 2: Each node in this layer is a fixed node which calculates the firing strength wi of a rule. The output of each node is the product of all the incoming signals to it and is given by,

$$O_i^2 = w_i = \mu_{A_i}(x) \times \mu_{B_i}(y), \quad i = 1, 2 \quad (41)$$

Layer 3: Every node in this layer is a fixed node. Each ith node calculates the ratio of the it rule's firing strength to the sum of firing strengths of all the rules. The output from the ith node is the normalized firing strength given by,

$$O_i^3 = \overline{w_i} = \frac{w_i}{w_1 + w_2}, \quad i = 1, 2 \quad (42)$$

Layer 4: Every node in this layer is an adaptive node with a node function given by

$$O_i^4 = \overline{w_i} f_i = \overline{w_i}(p_i x + q_i y + r_i), \quad i = 1, 2 \quad (43)$$

where$\overline{wi}$ is the output of Layer 3 and {pi, qi, ri} is the consequent parameter set.

Layer 5: This layer comprises of only one fixed node that calculates the overall output as the summation of all incoming signals, i.e.

$$O_i^5 = overall\ output = \sum_i \overline{w_i} f_i = \frac{\sum_i w_i}{\sum_i u} \quad (44)$$

(D) Learning Algorithm

In the ANFIS structure, it is observed that given the values of premise parameters, the final output can be expressed as a linear combination of the consequent parameters. The output f in Fig. 8 can be written as

$$\begin{aligned} f &= \frac{w_1}{w_1 + w_2} f_1 + \frac{w_2}{w_1 + w_2} f_2 \\ &= \overline{w_1}\, f_1 + \overline{w_2}\, f_2 \\ &= (\overline{w_1}\, x) p_1 + (\overline{w_1}\, y) q_1 + (\overline{w_1}) r_1 + (\overline{w} \end{aligned} \quad (45)$$

Where f is linear in the consequent parameters (p_1, q_1, r_1, p_2, q_2, r_2).

In the forward pass of the learning algorithm, consequent parameters are identified by the least squares estimate. In the backward pass, the error signals, which are the derivatives of the squared error with respect to each node output, propagate backward from the output layer to the input layer. In this backward pass, the premise parameters are updated by the gradient descent algorithm.

(VI) SIMULATION RESULTS

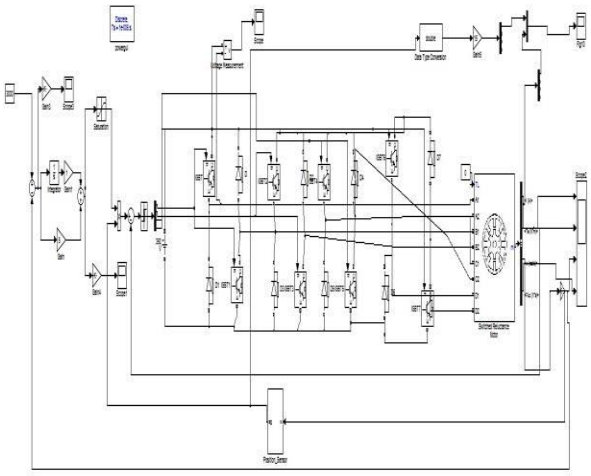

Fig.9.Simulink Diagram **o**f Existing System

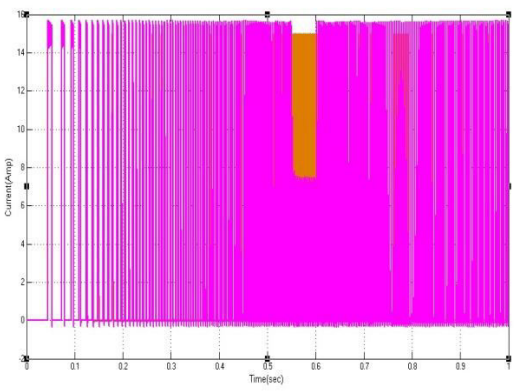

Fig.10. Phase current and its reference with proposed current controller at 1000 r/min

Fig.10 shows the phase current waveform and its reference. As a comparison, hysteresis current

International Journal For Advanced Research In Science & Technology
A peer reviewed international journal
www.ijarst.in
ISSN: 2457-0362

control with hysteresis band of ±0.5A is applied on the same SRM model. The sampling rate of the hysteresis controller is set to 100 kHz. Since the hysteresis controller is digitally implemented, one-sample-time delay is taken into account.

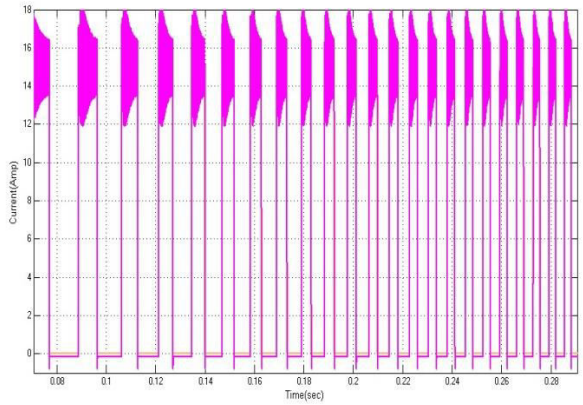

Fig. 11. Phase current and its reference with hysteresis current controller at 1000 r/min

Fig. 11 shows the phase current and its reference. It is shown that the proposed current controller has almost the same dynamic response and accuracy compared with hysteresis controller. Even though the hysteresis current controller has a very narrow hysteresis band and very high sampling rate, due to the finite sampling rate and the one-sample-time delay, the current ripples are still larger than that of the proposed controller.

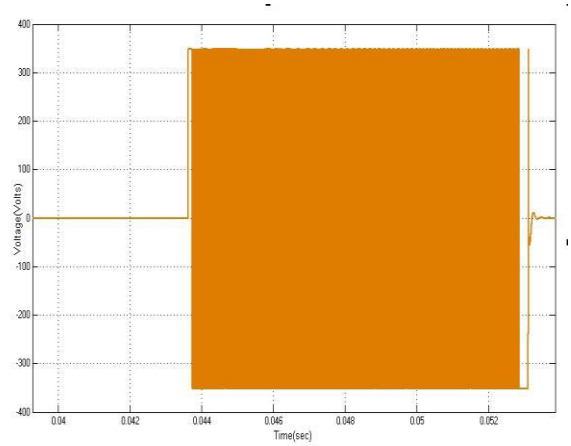

Fig.12.Calculated $u_c$of one phase during the simulation at 1000 r/min.

Fig. 12 shows the calculated uc by the proposed controller. It is shown that due to the nonlinearity of SRM, uc is very nonlinear. This also indicates the proposed controller has very high bandwidth.

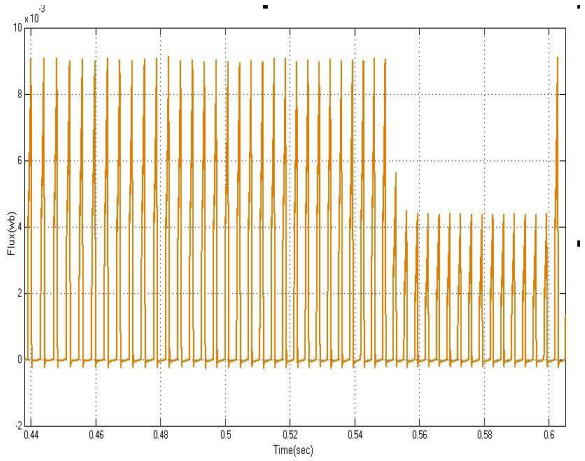

Fig .13(a). Waveforms of control error(e)

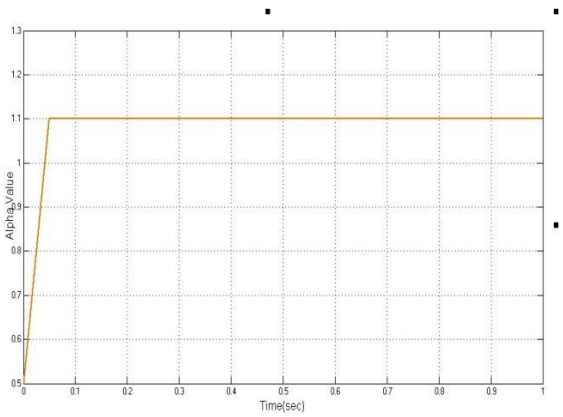

Fig 13(b). Waveforms of control Alpha(α)

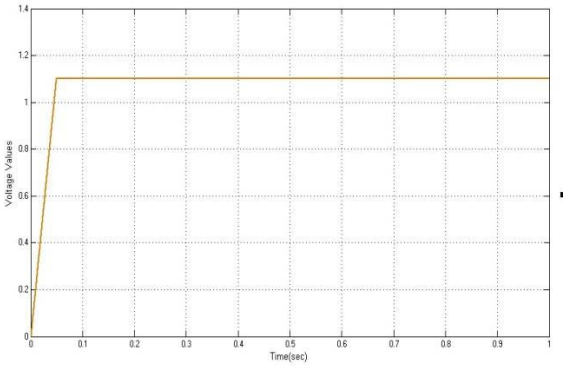

Fig 13 (c). Waveforms of control $v\hat{}$

International Journal For Advanced Research In Science & Technology
A peer reviewed international journal
www.ijarst.in
ISSN: 2457-0362

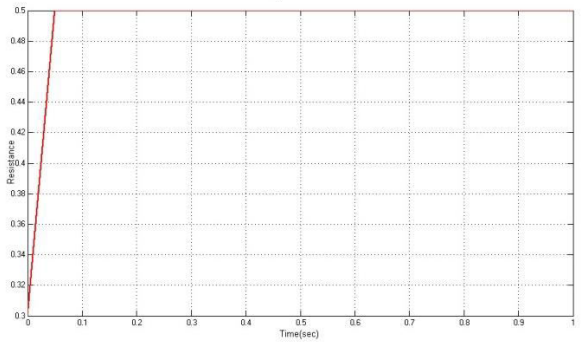

Fig 13 (d). Waveforms of control *R*

Fig. 13(a,b,c,d) shows the waveforms of control error(e), αˆ, Rˆ, and vˆ. It is shown that the control error is large due to the mismatch of parameters in the beginning. After the convergence of the parameters, the control error is greatly reduced.

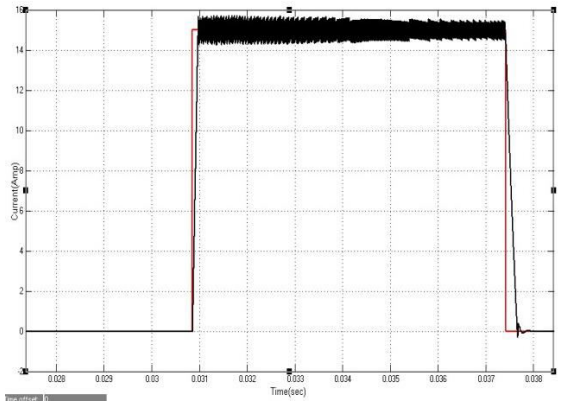

Fig.14: Phase current, current reference, the original flux linkage reference $\psi m(\theta, i\text{ref})$, and the adjusted flux linkage reference $\psi\text{adj}(\theta, i\text{ref})$ at 6000 r/min. (a) Phase current and its referencewith proposed current controller at 6000 r/min

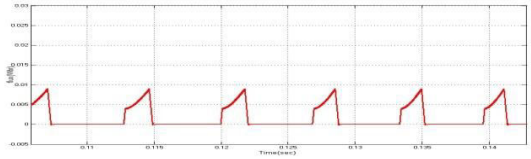

Fig.15: Phase current, current reference, the original flux linkage reference $\psi m(\theta, i\text{ref})$, and the adjusted flux linkage reference $\psi\text{adj}(\theta, i\text{ref})$ at 6000 r/min. (b) Original flux linkage reference $\psi m(\theta, i\text{ref})$, and the adjusted flux linkage reference $\psi\text{adj}(\theta, i\text{ref})$ at 6000 r/min

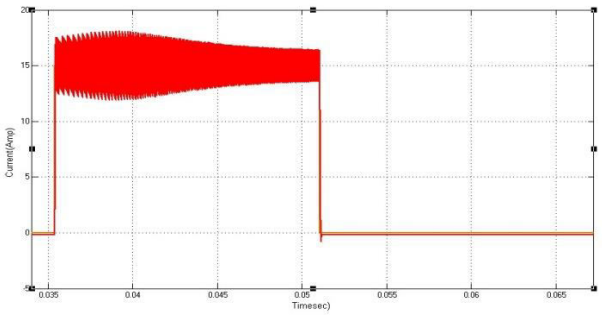

Fig16: Phase currents and its reference with hysteresis current controller at 6000 r/min.

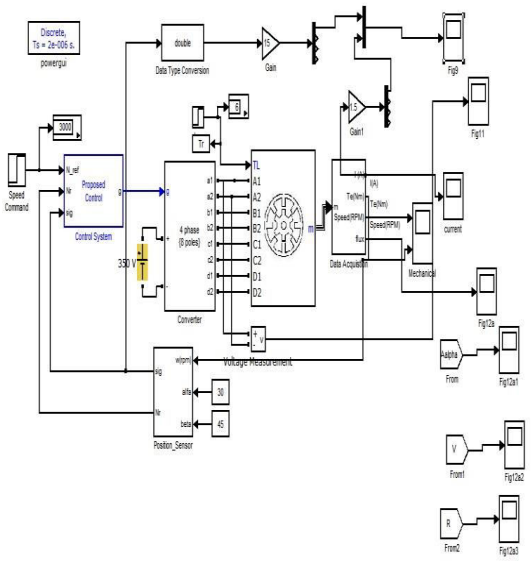

Fig 17:Simulink Diagram of Proposed System

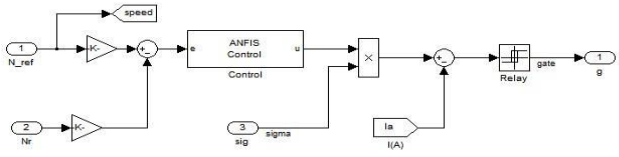

Fig 18:Simulink Diagram of Proposed System Controller

International Journal For Advanced Research In Science & Technology
A peer reviewed international journal
www.ijarst.in
ISSN: 2457-0362

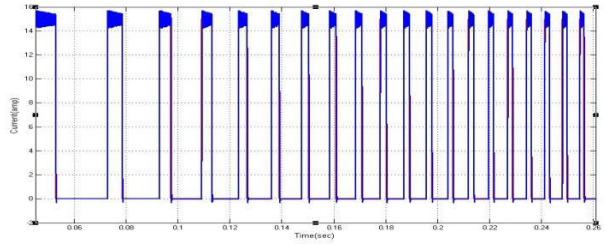

Fig.19: Phase current and its reference with Proposed current controller at 1000 r/min in ANFISController

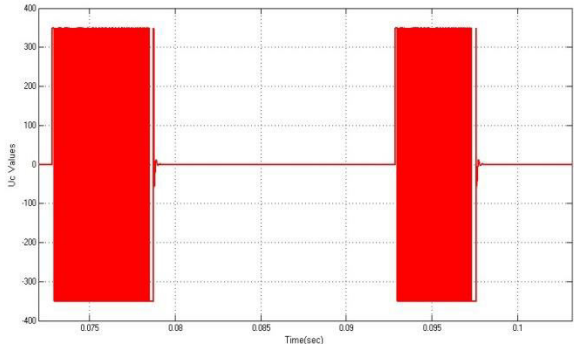

Fig.20: Calculated uc of one phase during the simulation at 1000 r/min.

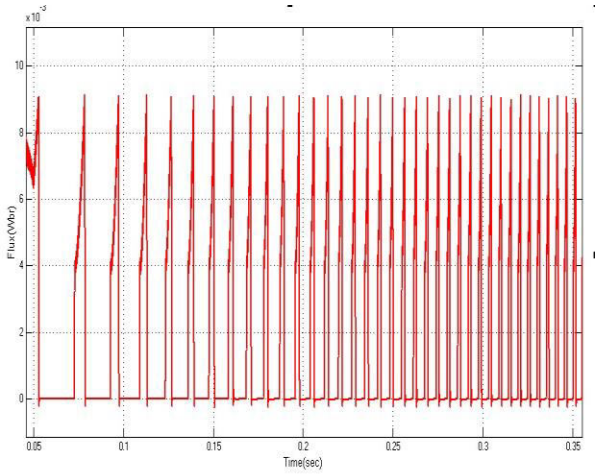

Fig.21: Waveforms of FLUX

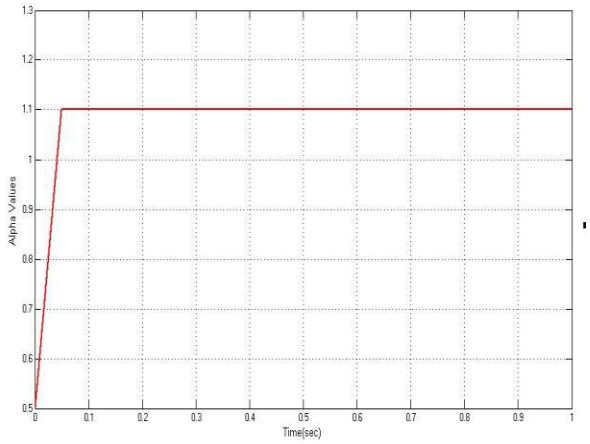

(A)

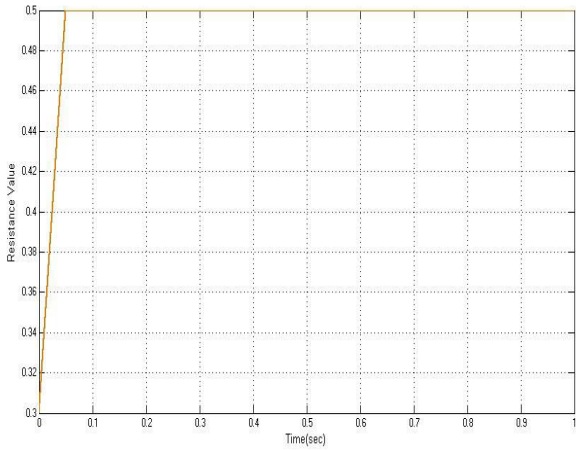

(B)

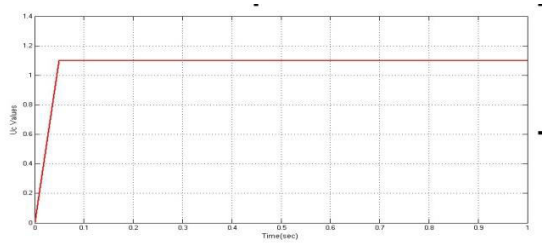

(C)

Fig 22: Waveforms of control error(e), αˆ, Rˆ, and vˆ.

VII. CONCLUSION

ANFIS based torque controller has been presented in this paperfor tractive application at low speeds. By using ANFIS controller,the SRM exhibits good

International Journal For Advanced Research In Science & Technology
A peer reviewed international journal www.ijarst.in
ISSN: 2457-0362

steady-state and dynamic performances. TheSRM can produce maximum torque quickly while needing shortduration overload ability.

REFERENCES

[1] A. Emadi, Energy-Efficient Electric Motors: Selection and Applications.New York, NY, USA: Marcel Dekker, Sep. 2004.

[2] J.-W. Ahn, S.-G. Oh, J.-W. Moon, and Y.-M. Hwang, "A three-phaseswitched reluctance motor with two-phase excitation," IEEE Trans. Ind.Appl., vol. 35, no. 5, pp. 1067–1075, Oct. 1999.

[3] J.-W. Ahn, S.-J.Park, and D.-H. Lee, "Hybrid excitation of SRM forreduction of vibration and acoustic noise," IEEE Trans. Ind. Electron.,vol. 51, no. 2, pp. 374–380, Apr. 2004.

[4] D.-H. Lee, Z.-G.Lee, and J.-W. Ahn, "Instantaneous torque control ofSRM with a logical torque sharing method," in Proc. IEEE Power Electron.Spec. Conf., Orlando, FL, USA, Jun. 2007, pp. 1784–1789.

[5] H. Goto, A. Nishimiya, H.-J.Guo, and O. Ichinokura, "Instantaneoustorque control using flux-based commutation and phase-torque distribution technique for SR motor EV," COMPEL: Int. J. Comput. Math.Electr.Electron. Eng., vol. 29, no. 1, pp. 173–186, Jan. 2010.

[6] J. Ye, B. Bilgin, and A. Emadi, "An extended-speed low-ripple torque control of switched reluctance motor drives," IEEE Trans. Power Electron.,vol. 30, no. 3, pp. 1457–1470, Mar. 2015.

[7] J. Ye, B. Bilgin, and A. Emadi, "An offline torque sharing function fortorque ripple reduction in switched reluctance motor drives," IEEE Trans.Energy Convers., vol. 30, no. 2, pp. 726–735, Jun. 2015.

[8] W. Cai and F. Yi, "An integrated multiport power converter with small capacitance requirement for switched reluctance motor drive," IEEE Trans.Power Electron., vol. 31, no. 4, pp. 3016–3026, Apr. 2016.

[9] F. Blaabjerg, P. Kjaer, P. Rasmussen, and C. Cossar, "Improved digitalcurrent control methods in switched reluctance motor drives," IEEE Trans.Power Electron., vol. 14, no. 3, pp. 563–572, May 1999.

[10] Y.-R. Mohamed and E. El-Saadany, "Robust high bandwidth discretetime predictive current control with predictive internal ModelAunifiedapproach for voltage-source PWM converters," IEEE Trans. Power Electron., vol. 23, no. 1, pp. 126–136, Jan. 2008.

[11] S. Schulz and K. Rahman, "High-performance digital PI current regulator for EV switched reluctance motor drives," IEEE Trans. Ind. Appl.,vol. 39, no. 4, pp. 1118–1126, Jul. 2003.

[12] B. Shao and A. Emadi, "A digital PWM control for switched reluctancemotor drives," presented at the IEEE Vehicle Power Propulsion Conf.,Lille, France, Sep. 2010.

[13] R. Cardenas, R. Pena, M. Perez, J. Clare, G. Asher, and P. Wheeler, "Control of a switched reluctance generator for variable-speed wind energyapplications," IEEE Trans. Energy Convers., vol. 20, no. 4, pp. 781–791,Dec. 2005.

[14] I. Husain and M. Ehsani, "Torque ripple minimization in switched reluctance motor drives by PWM current control," IEEE Trans. Power Electron.,vol. 11, no. 1, pp. 83–88, Jan. 1996.

[15] H. Vasquez and J. K. Parker, "A new simplified mathematical model fora switched reluctance motor in a variable speed pumping application,"Mechatronics, vol. 14, no. 9, pp. 1055–1068, Nov. 2004.